RSC Advances

ROYAL SOCIETY OF CHEMISTRY

www.rsc.org/advances

Facile fabrication of flower-like CuO/$Cu(OH)_2$ nanorods film with tunable wetting transition and excellent stability

*Weitao Liang, Liqun Zhu, Weiping Li, Huicong Liu**

Key Laboratory of Aerospace Materials and Performance (Ministry of Education), School of Materials Science and Engineering, Beihang University, Beijing 100191, China

Corresponding Author

Huicong Liu

Key Laboratory of Aerospace Materials and Performance (Ministry of Education), School of Materials Science and Engineering, Beihang University, Beijing 100191, China

*E-mail address: liuhc@buaa.edu.cn

Tel: +86 1082317113. Fax: +86 1082317133.

Abstract

Flower-like CuO/$Cu(OH)_2$ nanorods film on brass substrate has been synthesized for the first time, with tunable wetting transition and excellent stability. We raised a facile etching method utilizing electrolyte containing $K_2S_2O_8$ and KOH in this paper. The growth process and the surface morphology of the flower-like CuO/$Cu(OH)_2$ nanorods are well studied. Besides, the surface wetting behavior is reversible between superhydrophilic and superhydrophobic. The as prepared superhydrophilic surface can be converted to superhydrophobic by modification with

the myristic acid, which can be changed back to superhydrophilic after annealing at 200 ^{o}C for 6 min. The wetting transition can be cycled for more than 30 times with less than 10 min per cycle. We also discussed the wetting transition mechanism based on the surface composition analysis and relevant theoretical model, and investigated the abrasion resistance and flush resistance. For the primary application, we propose a water drop collecting device based on the large-scale and complex superhydrophobic surface would show excellent performance.

Keywords: smart surface, alternating current, superhydrophobic, tunable wetting transition, water collecting

1. Introduction

In recent years, surperhydrophobic surface (with water contact angle larger than 150^{o}) and superhydrophilic surface (with water contact angle less than 5^{o}), two important forms of the solid surface, have attracted extensive attention for potential applications[1-7]. Furthermore, the smart surfaces with tunable transition between the superhydropphobicity and superhydrophilicity have been investigated by lots of people[8-11] due to the numerous industrial applications in antifogging surfaces[12], self-cleaning coatings[13-15], oil-water separation[16], microfluid manipulation[17], biotechnology[18], etc. Many methods are employed to fabricate this smart surface, such as anodic oxidation, electrodeposition, plasma etching, dip coating, hydrothermal, electrospinning, sol-gel processing, and laser irradiation[19-26]. However, these surfaces are fabricated on expensive substrates and demand strict reaction conditions, which greatly limit their applications.

Our group has committed to study the controllable wetting behavior for a few years[27-29]. In our previous work, controllable superhydrophobic and superhydrophilic surface has been fabricated on brass substrate (an alloy of Cu and Zn) by an alternating current (AC) etching method in an acidic solution[29]. Brass is widely used in industrial applications for the good performance and low price. AC etching is also facile and suitable. However, the prepared pine-cone structure was attained by decomposition of Zn without further reaction, which makes the products uneven and large-size (about hundred nanometers to several micrometers). The large-size structure presents bad property in abrasion resistance and flush resistance test, which greatly limit its application potential.

In this study, the easy and suitable alternating current (AC) etching method is employed to fabricate tunable surface between superhydrophobicity and superhydrophilicity on brass

substrate in an alkaline solution with etching duration of 15 min under 20 V AC voltage. According to the results of the contact angles test, this surface is superhydrophilic. After modification by myristic acid (CH_3-$(CH_2)_{12}$-COOH) for 30s, the superhydrophilic surface transforms to superhydrophobic. After annealing at 200 ^oC for 6 min, the surface returned to the superhydrophilic again. Furthermore, this modification and annealing process can be cycled more than 30 times with good performance. And the whole wetting transition cycle cost a less time of 10 min. Different from the method of Wang's[29], the fabrication process in this work contains two steps, decomposition of Zn and oxidation of the left Cu. The further oxidation of Cu results in the uniform and smaller size nanorods, which greatly improve the stability of the prepared surface and extend applications. It's mainly because the decomposition reaction is strong and uncontrollable, while the oxidation process is more gentle and specific. As a preliminary application, a water drop collecting device based on the surperhydrophobic surface is suggested and a better performance is expected.

2. Experimental details

2.1 Materials

KOH, $K_2S_2O_8$, acetone, ethanol and myristic acid (CH_3-$(CH_2)_{12}$-COOH) were of analytical grade without further treatment. Brass substrates containing 64 wt % Cu and 36 wt % Zn and an aqueous electrolyte solution containing KOH and $K_2S_2O_8$ were used. Before the etching, the brass substrate was ultrasonically cleaned in acetone and then polished by sandpaper and rinsed by deionized water and ethanol in sequence.

2.2 Fabrication of the flower-like $CuO/Cu(OH)_2$ nanorods

At the beginning of the AC etching, two polished brass substrates were immersed in the prepared aqueous solution as electrodes. Then an AC voltage (20 V and 50 Hz) was applied to the two electrodes for a series of time of 1min, 5min, 10min, 15min, 20min, 30min. The electrolyte solution contained 0.025M $K_2S_2O_8$ and 1.0 M KOH and the etching temperature was kept at 50 ^oC by a water bath. The agitation rate was 600 r/min. At last, the two brass substrates were taken out and rinsed with deionized water and ethanol in sequence.

2.3. Wetting transition cycle

To fabricate the superhydrophobic surface, 0.48 g myristic acid was dissolved in 500 ml ethanol to modify the obtained brass substrate surface. The prepared substrate was immersed in the solution for 30s at the home temperature. After picked out of the solution, the prepared substrate was dried in room temperature and then a superhydrophobic surface was obtained.

After annealing at 200^oC for several minutes, the superhydrophobic surface converted into the superhydrophilic surface fast, and the appropriate annealing time was tested. By repeating the previous modification step, the annealed surface returned to superhydrophobicity again. Further annealing also can make it superhydrophilic. This transition cycle can be repeated more than 30 times with a stable wetting behavior.

2.4. Characterizations

A scanning electron microscope (SEM, JSM-7500F, JEOL Ltd., Japan) was used to observe the surface morphology of the obtained flower-like nanorods. Before the observation, the samples were sputter-coated with Pt under the vacuum conditions for electric conduction. The crystallographic characterization was investigated by X-ray diffractometer (XRD, ARL XTRA,

Themo Electron CO., Switzerland) with Cu K radiation at a scan speed of 6^o/min in the 2 range from 5^o to 90^o. To study the surface composition, an X-ray photoelectron spectroscopy (XPS; VG Scienific ESCA-LAB 250) with 200 W AL K radiation was used. Transmission electron microscopy (TEM; JEM-2100M) was used to evaluate the microstructure of the prepared substrate. The digital photographs were obtained by a digital camera (Olympus E-PL1, Japan). The contact angles were measured using a contact angle meter (DSA 20, Krüss Instruments GmbH) on five different positions for each surface. The volume of an individual droplet in all measurements was about 6 μL.

3. Results and discussion

3.1. Formation of the flower-like $CuO/Cu(OH)_2$ nanorods

To better observe the formation of flower-like $CuO/Cu(OH)_2$ nanorods, the SEM images of the growth process are shown in Figure 1. Figure 1 (A) shows the bare brass substrate before AC etching. It's rough with clearly scratches due to the mechanical polishing. The XRD pattern in the Figure 2 (a) shows that the brass substrate is composed of 64 wt% Cu and 36 wt% Zn. With increasing AC etching time to 1 min, the surface morphology of the brass substrate changed dramatically. Particles ranging from hundreds of nanometers to several micrometers observed on the surface due to the release of the Zn, as shown in Figure 1 (B). Zn would preferentially be oxidized to Zn^{2+} because it is more active than Cu[30]. As time increased to 5 min, more Zn decomposed. By the way, some small crystals with a size of few nanometers can be observed on the left particles, which were the first generation of $CuO/Cu(OH)_2$, as shown in Figure 1 (C). The irregular particles with first generated $CuO/Cu(OH)_2$ disappeared when the etching time increased to 10 min due to the further decomposition of the Zn. The solution also became turbid

with the decomposition of Zn. Crystals with 200 nm in diameter lay on the surface , which can be confirmed as mainly Cu by EDS, as shown in Figure 1 (D) (the peak on the right is corresponding to Pt sputter-coated before). These crystals were stable and provided appropriate places for $CuO/Cu(OH)_2$ to grow. Small nanorods can be observed in Figure 1 (D), which is the prototype of the flower-like nanorods. Figure 1 (E) and (F) show the surface morphology and the high-resolution image of the brass substrate after etching for 15 min. The prepared $CuO/Cu(OH)_2$ nanorods with a diameter of about 20 nm and a length of about 200 nm lay on the surface uniformly. The prepared $CuO/Cu(OH)_2$ nanorods marked by white pane in Figure 1 (F) presented a flower-like and uniform morphology. Figure 1 (G) shows the surface morphology after etching for 20 min. Some of the prepared nanorods film destroyed with the further decomposition of Zn while some of them left on the surface (marked by white arrow in Figure 1 (G)). New nanorods generated on the new exposed Cu and the surface morphology became uneven with mixed structures. As etching time increased to 30 min, the nanorods further fell off from the surface, as shown in Figure 1 (H). The brass substrate surface completely lost its flower-like morphology. Above all, the AC etching time of 15 min is appropriate. (The effects of the different KOH and $K_2S_2O_8$ concentration, on the morphology of the prepared nanorods, were also shown in Supporting Information Figure S1 and S2. A contrast experiment without the AC current with other experimental condition was carried out and the result was shown in Supporting Information Figure S3)

Figure 2 (A) shows the TEM image of the prepared nanorods. The rectangle area is about 400 nm × 600 nm and it contains tens of nanorods and nano particles which from the grinding. The nanorods with diameters of about 20 nm and length of about 200 nm can be observed clearly in the TEM image, which conformed to the SEM image shows before (Supporting Information

Figure S4). Figure 2 (B) is the high-resolution TEM image of the region marked by white arrow in Figure 2 (A), showing a lattice fringe of 0.252 nm, which is matched to the CuO (002) lattice spacing. Figure 2 (C) is the electron diffraction pattern of the area marked by the white arrow in Figure 2 (A), which shows various index facets of the marked area. Lattice spacing of 0.252 nm, 0.232 nm and 0.150 nm can be observed, which corresponding to the (002), (111) and (113) planes, respectively, of the phase CuO (PDF 45-0937). Besides, we can also find lattice spacing of 0.263 nm, 0.208 nm, 0.193nm and 0.172nm, which are corresponding to $Cu(OH)_2$ (PDF35-0505) phases of (002), (131), (112) and (132), respectively. The Figure 2 (D) shows the XRD patterns of the pure brass substrates and after AC etching treatment for 15 min. As stated in Figure 2 (D) (a), the peaks at 42.3°, 49.3°, 72.2° and 87.5° match well with the diffraction peaks of $Cu_{0.64}Zn_{0.36}$ (PDF No.50-1333), which indicates that the brass substrate is composed of 64 wt % Cu and 36 wt % Zn. The emergence of peaks at 35.5° and 38.7° in the Figure 2 (D) (b) indicates that CuO (PDF No.45-0937) appears on the brass substrate surface after AC etching for 15 min. Meanwhile, the existence of peaks at 31.5°, 34.1°, 35.9°, 43,5° and 53.3° match well with the diffraction peaks of $Cu(OH)_2$ (PDF=35-0505), which indicates that $Cu(OH)_2$ appears after the AC etching. In addition, we can also find significant peaks of $Cu_{0.64}Zn_{0.36}$ in the Figure 2 (D) (b), which indicates that the CuO/$Cu(OH)_2$ film is thin and this is consistent with the SEM analysis results. The results of TEM and XRD analyze further confirm the existence of CuO/$Cu(OH)_2$.

From what has been discussed above, we conclude that the whole process of the flower-like CuO/$Cu(OH)_2$ nanorods formation as follows[31]:

Instant anode: $Zn + 4OH^- - 2e^- \longrightarrow Zn(OH)_4^{2-}$ (1)

Instant cathode: $2H_2O + 2e^- \longrightarrow 2OH^- + H_2 \uparrow$ (2)

Secondary reaction: $Cu + S_2O_8^{2-} + 2OH^- \longrightarrow Cu(OH)_2 \downarrow + 2SO_4^{2-}$ (3)

$$Cu(OH)_2 \longrightarrow CuO + H_2O \quad (4)$$

The Figure 3 shows the mechanism of the AC etching of brass substrate in solution containing KOH and $K_2S_2O_8$. In the AC etching duration, the two brass substrates serve as the anode and cathode alternately and both of the brass substrates would be covered with flower-like $CuO/Cu(OH)_2$ nanorods at last. That is, we can fabricate two products at the same time.

At the beginning of the AC etching, the Zn in the brass substrate reacted with OH^- for it is amphoteric metal and more active than Cu[30], as shown in Eq. (1), which is called "dezincification". The Zn gradually dissolved in solution and the Cu was left on the surface of the substrate. This "dezincification" process is same with the method in our previous work[29], while the products are different for the different reaction conditions. In this work, after the "dezincification", the left Cu can be easily oxidized by $S_2O_8^{2-}$ with the existence of OH^- and turn into $Cu(OH)_2$[11], as shown in Eq. (3). $Cu(OH)_2$ is not stable and can decompose into CuO and H_2O under high temperature, as shown in Eq.(4). The AC etching method released a great deal of thermal energy and further accelerated the decomposition of $Cu(OH)_2$. Thus the new generated nanorods are mixture of CuO and $Cu(OH)_2$. Some of the left Cu grains with new generated $CuO/Cu(OH)_2$ on it would dissolve simultaneously with Zn[32] and mixed into the solution, which made the solution turbidity as described above. The new $CuO/Cu(OH)_2$ would grow on the new exposed Cu grains. This process would continue until the left Cu grains can stay on the surface stable, as shown in the Figure 1 (D), which will take about 15 min. Then the new generated

$CuO/Cu(OH)_2$ can grow into uniform nanorods with flower-like structure, as shown in the Figure 1 (E) and (F). The prepared $CuO/Cu(OH)_2$ nanorods are more uniform and smaller than the pine-cone structure in our previous work for the oxidation process is softer than the decomposition. As time goes on, more Zn grains dissolved in the solution and the generated $CuO/Cu(OH)_2$ nanorods film was destroyed, as shown in the Figure 1 (G) and (H). We can also find that the left $CuO/Cu(OH)_2$ nanorods in the Figure 1 (G) (marked by the white arrow), which further validated our speculation.

3.2. Wetting transition between the superhydrophobicity and superhydrophilicity.

The as-prepared surface was superhydrophilic with a contact angle less than 3^o, as shown in Figure 4 (A). After immersing in the myristic acid ethanol solution for 30s and drying at room temperature for several min, the surface converted to superhydrophobic, as shown in Figure 4 (B). By comparing the SEM images before and after modification shown in Figure 4 (A) and (B) we can find that the surface morphology has no apparent change and still composed of flower-like nanorods. After annealing at 200 ^oC for several minutes, the contact angle returned to less than 3^o without apparent surface morphology change, as shown in Figure 4 (C). It indicates that the modification and annealing do not change the surface morphology and the change of wetting behavior is mainly because the modification of the myristic acid and annealing. The myristic acid combined with the surface during the immersing process and the "combination" was damaged during the annealing, which cause the wetting behavior changing between superhydrophilicity and superhydrophobicity, as shown in Figure 4 (D). (The digital images of CAs of the modified surfaces with different AC etching durations are shown in Supporting Information Figure S5. Digital photographs of the process of modified surface contact the water droplet are shown in Supporting Information Figure S6.)

It's known that chemical composition and microstructure are the key factors influencing the wetting behavior of a solid surface[33, 34]. The phenomenon stated above indicates that the superhydrophobicity of the substrate is governed by both the flower-like nano structure and the low surface energy materials. The contrast experiments about CAs on blank brass substrate and modified brass substrate were also carried out and the result was shown in Figure 5. The blank brass is hydrophilic with CA of 68±1.0^o and the modified blank brass is hydrophobic with CA of 95±1.2^o. The blank brass is hydrophilic because the hydroxyl group is absorbed on the metal surfaces. After modification with myristic acid, the CAs increased for the myristic acid combination on the surface and stop the hydroxyl group from absorbing on the metal surface. The figure 5 (C) and (D) show that the prepared CuO/Cu(OH)$_2$ nanorods film substrate is superhydrophilic with CA of 0^o and the modified substrate is superhydrophobic with CA of 162±2.1^o, this can be also contributed to the combination of the myristic acid on the surface. According to the previous work[29, 35, 36, 37], the combination between CuO/Cu(OH)$_2$ and myristic acid can be concluded as follows:

$$CuO + 2CH_3(CH_2)_{12}COOH \leftrightarrow Cu[\ CH_3(CH_2)_{12}COO\ ]_2 + H_2O \quad (5)$$

$$Cu(OH)_2 + 2CH_3(CH_2)_{12}COOH \leftrightarrow Cu[\ CH_3(CH_2)_{12}COO\ ]_2 + 2H_2O \quad (6)$$

CuO and Cu(OH)$_2$ are prone to react with the myristic acid in the ethanol solution[11, 29, 36], so the myristic acid group will react with CuO/Cu(OH)$_2$ and form the Cu[CH$_3$(CH$_2$)$_{12}$COO]$_2$ on the surface of the prepared CuO/Cu(OH)$_2$ nanorods film. The surface after modification is superhydrophobic for the Cu[CH$_3$(CH$_2$)$_{12}$COO]$_2$ is low surface energy material with long-chain aliphatic groups. During the annealing process, the long-chain aliphatic groups are damaged and the surface turns into superhydrophilic. Besides, the "combination" between myristic acid and

pure brass substrate in Figure 5 (B) can be also attributed to the formation of $Cu[CH_3(CH_2)_{12}COO]_2$ and $Zn[CH_3(CH_2)_{12}COO]_2$ for the similar reactions[29,36, 37].

According to the Cassie-Baxter model[38] shown as follows:

$$\cos\theta_r = f_1\cos\theta - f_2 \quad (7)$$

$$f_1 + f_2 = 1 \quad (8)$$

Where θ_r represents the contact angle on the rough surface, θ represents the contact angle on the smooth surface, f_1 and f_2 are the fraction of the solid surface and air trapped in grooves when contacting with water, respectively. It can be easily known that f_1 plus f_2 is 1, as shown in the Eq. (8). According to the result of the contact angles test, the θ_r after modification was 162 ± 2.1^o and the CAs of the modified smooth brass substrate surface was 95 ± 1.2^o (shown in Figure 5 (B)), which can be considered as θ[39]. By putting them into the Eq. (7), the values of the f_1 and f_2 can be calculated to be 0.0537 and 0.9463, respectively. The results mean that air occupies about 94.63 % of the contact areas when the modified prepared surface contact with the water droplet. It is because the 3D capillary effect of the prepared CuO nano-structure provides more space for trapping air, which greatly increase the air/liquid interfaces, just as shown in the Figure 4 (D). The modification of the low surface energy materials makes the interaction force lower to further improve the sperhydrophobicity of the prepared surface.

Above all, the whole transition process can be concluded as follows: A rough surface with high energy materials tends to be hydrophilic and a rough surface with low energy materials tends to be hydrophobic. The as-prepared nanorods film is superhydrophilic for it is high surface energy material and the hydroxyl group can be easily absorbed on the surface. After modification

of myristic acid, the $CuO/Cu(OH)_2$ react with the myristic acid and produce $Cu[CH_3(CH_2)_{12}COO]_2$, which is low surface energy material with long-chain aliphatic group. The nanorosd film with hierarchical nano-structure and $Cu[CH_3(CH_2)_{12}COO]_2$ on it show superhydrophobic property. After annealing at 200 ^oC, the long-chain aliphatic group has decomposed and the surface return into superhydrophilic. The remodification process can form new long-chain aliphatic groups and the surface turn into suprhydrophobicity again. The modification and annealing process would not affect the morphology of the prepared surface, thus this wetting transition can be cycled many times.

As stated above, the wettability of the solid surface depends on the surface morphology and low surface energy materials. In this study, the superhydrophobicity was achieved by modification of the prepared flower-like $CuO/Cu(OH)_2$ nanorods with myristic acid. To remove the low surface energy materials, the modified substrate was annealed at 200 ^oC. To find the appropriate time of annealing, the contact angles of the prepared surface after different annealing time were measured, as shown in Figure 6 (A). The results illustrate that as annealing time prolonged, the contact angles of the prepared surface decreased and after annealing for 6 min, the contact angle came to zero. That is, the superhydrophobic surface became superhydrophilic surface after annealing and 6 min is long enough for this transition. To immerse the annealed substrate into myristic acid ethanol solution for 30 s again, the surface will recovered to superhydrophobicity after drying at room temperature. By further experiment, this wettability change was cycled several times to confirm its stability. The experimental results shown in Figure 6 (B) indicate a good reversibility of the wettability. In fact, after 30 cycles, the prepared surface can also keep excellent reversibility in this experiment, which is longer than those reported surfaces[4, 10, 39, 29, 40-44]. This can be attributed to the smaller size of the nanorods, which

is not easy to be damaged and make the surface more stable. It's obvious that the longer the wettability cycling lasts, the wider its application will be. In this word, the new prepared surface has great potential in practical applications. In addition, each cycle of the wettability change in this study takes less than 10 min, which is much shorter than reported before.

3.3. Component analysis of the surfaces.

From stated above we know that the modification and annealing do not change the surface morphology and the change of wetting behavior is mainly because the combination and release of the myristic acid on the surface. To confirm this viewpoint, the X-ray photoelectron (XP) spectra of the prepared surfaces before modification of myristic acid (which is called the blank sample), after modification of myristic acid (modified sample) and after annealing at 200 ^{o}C (annealed sample) were carried out and showed in Figure 7, which can further illustrate the surface composition of the three different states. The results of the XPS survey spectra in the Figure 7 (a) indicate that Cu, O and C can be detected on the three surfaces. Figure 7 (b) shows the high-resolution of Cu 2p regions, in which we can find typical Cu 2p spectrum. The blank sample and modified sample present obvious peaks at 933.4 and 934.4 eV, which are corresponding to CuO and $Cu(OH)_2$, respectively. The Cu 2p intensity of blank sample is higher than modified sample for the modification. After annealing, the increase of peak at 933.7 eV indicates the increase of CuO. The result demonstrates that the $Cu(OH)_2$ is further decomposed during the thermal treatment. High-resolution spectrums of O 1s are also shown in Figure 7 (c). The blank sample contains the main peaks of CuO at 529.4 eV and $Cu(OH)_2$ at 531.7 eV, indicates that the prepared surface are mainly composed of CuO and $Cu(OH)_2$. An obvious peak at 533.3 eV appears after modification, corresponding to O-C=O, which indicates that the myristic acid adsorbed on the blank sample during the modification and produced

$Cu[CH_3(CH_2)_{12}COO]_2$ as stated above. After annealing, the peak stands for O-C=O also can be find, which indicates some $Cu[CH_3(CH_2)_{12}COO]_2$ left among the thermal treatment. High-resolution spectrum of O 1s of annealed sample in Figure 7 (c) shows that the main peaks of CuO at 529.4 eV increased after annealing, which further confirm the decomposition of $Cu(OH)_2$. Figure 7 (d) shows the high-resolution XPS spectra of the C 1s. After modification, obvious peaks at 288.5 and 284.6 eV appear on the graph, corresponding to O-C=O and C-C, which is attributed to the existence of $Cu[CH_3(CH_2)_{12}COO]_2$. After annealing, the C 1s peak intensity declines obviously, which due to the $Cu[CH_3(CH_2)_{12}COO]_2$ decomposed during the thermal treatment. Comparing modified sample and annealed sample indicating that although most of the $Cu[CH_3(CH_2)_{12}COO]_2$ is decomposed in the thermal treatment, some peaks of C 1s also can be observed, which is consistent with the O 1s analysis.

Table 1 also presents the surface composition of the blank sample, modified sample and annealed sample detected by XPS. The increase of C from 33.74% to 76.47% after modification by myristic acid implies that integral aliphatic group forms on the blank sample surface during the modification process. After annealing at 200 ^oC, the amount of C reduces from 76.47% to 32.33%, which indicates the decomposition of long-chain aliphatic group. This is consistent with the results of XPS analysis.

By further analysis we know that after annealing, the $Cu[CH_3(CH_2)_{12}COO]_2$ decomposed but the residual carbon can also adhere to the surface or just stay on the surface by physical adsorption[29, 45]. Even so, the wetting behavior of the prepared surface is less influenced by the residual carbon from the CAs test results in Figure 6 (B). It's mainly because most of the long-chain aliphatic group has decomposed due to the thermal treatment and new integral long-chain aliphatic group will be introduced on the surface after the remodification.

3.4. Abrasion resistance test and flush resistance test.

To further observe the abrasion resistance of the prepared superhydrophobic surface, a scratch test was carried out with 800# SiC sandpapers served as abrasive surfaces[46]. The prepared superhydrophobic surface to be tested was faced with the rough side of the sandpaper. A 50 g load was applied on the superhydrophobic surface and then the surface was moved 10 cm on the sandpaper longitudinally and transversely, which was defined as an abrasion cycle. Table 2 shows the change in the surface morphology and contact angle after 2 abrasion cycle. Water contact angle changed slightly within 15 cycles and then decreased gradually. The sample with 20 times abrasion test was re-modified by immersing in the myristic acid ethanol solution and the CAs were measured to be 146±1.9^{o}, which indicates that the micro/nano structure of the superhydrophobic surface was slightly damaged during the abrasion test. Even so, water droplets could easily roll off by a small sliding angle after being scratched repeatedly. It indicates that the prepared superhydrophobic surfaces possessed good abrasion resistance. (Schematic illustration is shown in Supporting Information Figure S7.)

A flush test was also carried out to further verify the stability of the superhydrophobic surface. The prepared surface was flushed by deionized water from 50 cm upon the surface at a speed of 5 mL per second[47]. After a continuous test of several hours, the sample was moved away to test the CAs at the place where the water flush on it to evaluate the flush resistance. The results in the table 3 shows that after a continuous flush test of about 6 hours, the CAs of the prepared surface can keep as high as 155±2.1^{o}, which indicates that the surface superhydrophobicity decreased in the duration of flush test, in spite of this, it still has excellent superhydrophobic performance. After continuous flush test of 12 hours, the superhydrophobicity is destroyed completely for the modified myristic acid has been flushed away. But by simple immersing in myristic acid ethanol

solution for 30 s and drying, the surface returned to superhydropholicity and also can keep more than 6 hours under flushing, which indicates that the flush test of 12 hours just flush away the modified myristic acid and didn't damage the nanostructures of the prepared surface. The results of the flush test indicate that the prepared superhydrophobic surface has a good performance in flush resistance. (Schematic illustration is shown in Supporting Information Figure S8.)

3.5. Further application potential.

The superhydrophobic materials are always required to be large and with complex shape in the practical industrial applications[48-50]. To meet the requirement, the AC etching method is also employed to fabricate large materials with complex shape. As shown in the Figure 8 (A) and (B), we fabricated a superhydrophobic surface on a large curved brass substrate (100mm × 50mm × 2mm), all the parameters are set up as described before. We can see many water droplets (10 μL) present round shapes with large CAs on the prepared surface, which indicates that the AC etching method of fabricating superhydrophobic surface can be successfully applied in large substrate with complex shape.

On the basis of the large complex shape superhydrophobic surface, a water drop collecting device is suggested to construct as the schematic diagram shown in Figure 8. The main working part is built by the prepared superhydrophobic substrate with a tilt of about 5^{o}, while the superhydrophobic surface towards the upside, as shown in Figure 8 (A). If there is a water drop falling on the surface of the collecting device, it will roll along the tilt direction for the small rolling angle, which is less than 3^{o}. The whole working process has been demonstrated in the Figure 8 (C), a water droplet falls on the superhydrophobic region and then rolls to the lower place for the small rolling angle. Finally, water droplets will collect together at the central and

flow into a container in case of drought and other useful place. This water drop collecting device should have a good performance and long service time for the excellent performance of the prepared superhydrophobic surface in abrasion resistance and flush resistance, and it will be very useful to collect water without energy in arid areas[51].

4. Conclusion

We demonstrate the fabrication of flower-like CuO/$Cu(OH)_2$ nanorods film on brass substrate by 20 V and 15 min alternate current etching method from $K_2S_2O_8$ and KOH aqueous solution. The flower-like nanorods with about 20 nm in diameter and a length of 200 nm stand on the brass substrate neatly and evenly with good performance in abrasion resistance and flush resistance. The superhydrophobicity is achieved by myristic acid modification. After annealing at 200 ^oC for 6 min, the superhydrophobic surface turns into superhydrophilicity. This tunable wetting transition can be realized by myristic acid modification and annealing for more than 30 cycles with a short time of 10 min each cycle. As a preliminary application, the prepared surface is suggested to construct a water drop collecting device. The prepared surface is expected to have potential applications in water collecting device, antifogging surfaces, self-cleaning coatings and so on.

Acknowledgment

The authors are very grateful to the support from the National Natural Science Foundation of China (Grant No. 51401011).

References

(1) Caputo, G.; Cortese, B.; Nobile, C.; Salerno, M.; Cingolani, R.; Gigli, G.; Cozzoli, P. D.; Athanassiou. Reversibly Light□Switchable Wettability of Hybrid Organic/Inorganic Surfaces With Dual Micro□/Nanoscale Roughness. A. Adv. Funct. Mater. 2009, 19, 1149-1157.

(2) Erbil, H. Y.; Demirel, A. L.; Avci, Y.; Mert, O. Transformation of a simple plastic into a superhydrophobic surface. Science. 2003, 299, 1377-1380.

(3) Feng, X. J.; Zhai, J.; Jiang, L. The fabrication and switchable superhydrophobicity of TiO_2 nanorod films. Angew. Chem., Int. Ed. 2005, 44, 5115-5118.

(4) Nishimoto, S.; Bhushan, B. Bioinspired self-cleaning surfaces with superhydrophobicity, superoleophobicity, and superhydrophilicity. Rsc Adv. 2013, 3, 671-690.

(5) Heikenfeld, J.; Dhindsa, M. J. Adhes. Electrowetting on superhydrophobic surfaces: present status and prospects. Sci. Technol. 2008, 22, 319-334.

(6) Roach, P.; Shirtcliffe, N. J.; Newton, M. I. Progess in superhydrophobic surface development. Soft Matter. 2008, 4, 224-240.

(7) Li, X. M.; Reinhoudt, D.; Crego-Calama, M. What do we need for a superhydrophobic surface? A review on the recent progress in the preparation of superhydrophobic surfaces. Chem. Rev. 2007, 36, 1350-1368.

(8) Pernites, R. B.; Ponnapati, R. R.; Advincula, R. C. Superhydrophobic–superoleophilic polythiophene films with tunable wetting and electrochromism. Adv. Mater. 2011, 23, 3207-3213.

(9) Hao, X. F.; Du, L. P.; Cai, H. G.; Zhang, C. Y.; Zhang, X. Q.; Zhang, H. X. Preparation of superhydrophobic cross-linked syndiotactic 1, 2-polybutadiene membranes by electrospinning. J. Nanosci. Nanotechnol. 2012, 12, 8077-8080.

(10) Wang, G.; Zhang, T.Y. Easy Route to the Wettability Cycling of Copper Surface between Superhydrophobicity and Superhydrophilicity. ACS Appl. Mater. Interfaces. 2012, 4, 273-279.

(11) Zhu, X.; Zhang, Z.; Men, X.; Yang, J.; Xu, X. Rapid formation of superhydrophobic surfaces with fast response wettability transition. ACS Appl. Mater. Interfaces. 2010, 2, 3636-3641.

(12) Introzzi, L.; Fuentes-Alventosa, J. M.; Cozzolino, C. A.; Trabattoni, S.; Tavazzi, S.; Bianchi, C. L.; Farris, S. "Wetting Enhancer" pullulan coating for antifog packaging applications. ACS Appl. Mater. Interfaces. 2012, 4, 3692-3700.

(13) Blossey, R. Self-cleaning surfaces—virtual realities. Nat. Mater. 2003, 2, 301-306.

(14) Xu, L.; He, J. Fabrication of highly transparent superhydrophobic coatings from hollow silica nanoparticles. Langmuir. 2012, 28, 7512-7518.

(15) Anandan, S.; Narasinga Rao, T.; Sathish, M.; Rangappa, D.; Honma, I.; Miyauchi, M. Superhydrophilic graphene-loaded TiO_2 thin film for self-cleaning applications. ACS Appl. Mater. Interfaces. 2012, 5, 207-212.

(16) Liang, W., Guo, Z. Stable superhydrophobic and superoleophilic soft porous materials for oil/water separation. RSC Adv. 2013, 3, 16469-16474.

(17) Cheng, Z.; Lai, H.; Zhang, N.; Sun, K.; Jiang, L. Magnetically Induced Reversible Transition between Cassie and Wenzel States of Superparamagnetic Microdroplets on Highly Hydrophobic Silicon Surface. J. Phys. Chem. C. 2012, 116, 18796-18802.

(18) Zhao, J.; Zhang, X.; Chen, N.; Pan, Q. Why Superhydrophobicity Is Crucial for a Water-Jumping Microrobot? Experimental and Theoretical Investigations. ACS Appl. Mater. Interfaces. 2012, 4, 3706-3711.

(19) Thieme, M.; Frenzel, R.; Schmidt, S.; Simon, F.; Henning, A.; Worch, H.; Lunkwitz, K.; Scharnweber, D. Generation of ultrahydrophobic properties of aluminium-A first step to self-cleaning transparently coated metal surfaces. Adv. Eng. Mater. 2001, 3, 691-695.

(20) She, Z. X.; Li, Q.; Wang, Z. W.; Li, L. Q.; Chen, F.N.; Zhou, J.C. Novel method for controllable fabrication of a superhydrophobic CuO surface on AZ91D magnesium alloy. ACS Appl. Mater. Interfaces. 2012, 4, 4348-4356.

(21) Tang, X.; Wang, T.; Yu, F.; Zhang, X., Zhu, Q.; Pang, L.; Zhang, G.; Pei, M. Simple, robust and large-scale fabrication of superhydrophobic surfaces based on silica/polymer composites. RSC Adv. 2013, 3, 25670-25673.

(22) Xu, L. B.; Karunakaran, R. G.; Guo, J.; Yang, S. Transparent, Superhydrophobic Surfaces from One-Step Spin Coating of Hydrophobic Nanoparticles. ACS Appl. Mater. Interfaces. 2012, 4, 1118-1125.

(23) Wang, C. F.; Tzeng, F. S.; Chen, H. G.; Chang, C. J. Ultraviolet-Durable Superhydrophobic Zinc Oxide-Coated Mesh Films for Surface and Underwater–Oil Capture and Transportation. Langmuir .2012, 28, 10015-10019.

(24) Bellanger, H.; Darmanin, T.; De Givenchy, E.T.; Guittard, F. Superhydrophobic hollow spheres by electrodeposition of fluorinated poly (3, 4-ethylenedithiopyrrole). RSC Adv. 2012, 2, 10899-10906.

(25) Yao, X.; Chen, Q.; Xu, L.; Li, Q.; Song, Y.; Gao, X.; David, Q.; Jiang, L. Bioinspired ribbed nanoneedles with robust superhydrophobicity. Adv. Funct. Mater. 2010, 20, 656-662.

(26) Shinde, S. L.; Nanda, K. K. Facile synthesis of large area porous Cu_2O as super hydrophobic yellow-red phosphors. RSC Adv. 2012, 2, 3647-3650.

(27) Wang, Z.; Zhu, L.; Li, W.; Liu, H. C. Superhydrophobic surfaces on brass with controllable water adhesion. Surf. Coat. Technol.2013, 235, 290-296.

(28) Wang, G.; Zhu, L.; Li, W.; Liu, H. C. Self-assembled biomimetic superhydrophobic $CaCO_3$ coating inspired from fouling mineralization in geothermal water. Langmuir. 2011, 27, 12275-12279.

(29) Wang, Z.; Zhu, L.; Li, W.; Liu, H. C. Rapid reversible superhydrophobicity to superhydrophilicity transition on alternating current etched brass. ACS Appl. Mater. Interfaces. 2013, 5, 4808-4814.

(30) Kwak, G.; Lee, M.; Yong, M. Chemically modified superhydrophobic WO_x nanowire arrays and UV photopatterning. Langmuir. 2010, 26, 9964-9967.

(31) Quan, L.; Zhu, L.; Li, W.; Liu, H. C. Fabrication of $Cu_{1.8}S$/CuS nanoplates counter electrode via alternating current etching for quantum dots-sensitized solar cells. RSC Adv. 2014, 4, 32214-32220.

(32) Joseph, G.; Arce, M. T. Contribution to the study of brass dezincification. Corros. Sci. 1967, 7, 597-605.

(33) Mumm, F.; van Helvoort, A. T. J.; Sikorski, P. Easy route to superhydrophobic copper-based wire-guided droplet microfluidic systems. ACS Nano. 2009, 3, 2647-2652.

(34) Wenzel, R. N. Surface roughness and contact angle. J. Phys. Chem. 1949, 53, 1466-1467.

(35) Kong, L.; Chen, X.; Yu, L.; Wu, Z.; Zhang, P. Superhydrophobic Cuprous Oxide Nanostructures on Phosphor-Copper Meshes and Their Oil-Water Separation and Oil Spill Cleanup. ACS Appl. Mate. Interfaces 2010, 2, 3636-3641.

(36) Li, G.; Chen, T.; Yan, B.; Ma, Y.; Zhang, Z.; Yu, T.; Shen, Z.; Chen, H.; Wu, T. Tunable wettability in surface-modified ZnO-based hierarchical nanostructures. Appl Phys Lett. 2008, 92, 173104.

(37) Li, J.; Yang, Y.; Zha, F.; Lei, Z. Facile fabrication of superhydrophobic ZnO surfaces from high to low water adhesion. Mater Lett. 2012, 75, 71-73.

(38) Cassie, A. B. D.; Baxter, S. Wettability of porous surfaces. Trans. Faraday Soc.1944, 40, 546-551.

(39) YanLong, S.; Wu, Y.; Jiajing, B.; XiaoJuan, F.; YongSheng, W. Fabrication of flower-like copper film with reversible superhydrophobicity-superhydrophilicity and anticorrosion properties. Surf. Coat. Technol. 2014, 253, 148-153.

(40) Caputo, G.; Nobile, C.; Kipp, T.; Blasi, L.; Grillo, V.; Carlino, E.; Manna, L.; Cingolani, R.; Cozzoli, P. D.; Athanassiou, A. Reversible wettability changes in colloidal TiO_2 nanorod thin-film coatings under selective UV laser irradiation. J. Phys. Chem. C. 2008, 112, 701-714.

(41) Chang, Y. H.; Hau, N. Y.; Liu, C.; Huang, Y. T.; Li, C. C.; Shih, K.; Feng, S. P. A short-range ordered–disordered transition of a NiOOH/$Ni(OH)_2$ pair induces switchable wettability. Nanoscale. 2014, 6, 15309-15315.

(42) Tavana, H.; Amirfazli, A.; Neumann, A. W. Fabrication of superhydrophobic surfaces of n-hexatriacontane. Langmuir. 2006, 22, 5556-5559.

(43) Zheng, Y.M.; L. Jiang.; Wang, J.X.; Han, D. Closed-air induced composite wetting on hydrophilic ordered nanoporous anodic alumina. Appl. Phys. Lett. 2008, 96, 094107.

(44) Mondal, C.; Ganguly, M.; Sinha, A. K.; Pal, J.; Pal, T. Fabrication of a ZnO nanocolumnar thin film on a glass slide and its reversible switching from a superhydrophobic to a superhydrophilic state. RSC Adv. 2013, 3, 5937-5944.

(45) Xin, B. W.; Hao, J. C. Reversibly switchable wettability. Chem. Soc. Rev. 2010, 39, 769-782.

(46) Lacombe R. Adhesion measurement methods: theory and practice. CRC Press. 2010.

(47) Kleinman, B.; Powell, S.; Kumar, P.; Gardner, R. M. The fast flush test measures the dynamic response of the entire blood pressure monitoring system. Anesthesiology. 1992, 77, 1215-1220.

(48) Acatay, K.; Simsek, E.; Ow-Yang, C.; Menceloglu, Y. Z. Tunable, superhydrophobically stable polymeric surfaces by electrospinning. Angew. Chem., Int. Ed. 2004, 43, 5210-5213.

(49) Aristoff, J. M.; Bush, J. W. M. Water entry of small hydrophobic spheres. J. Rev. Fluid Mech. 2009, 619, 45-78.

(50) Bush, J. W. M.; Hu, D. L. Walking on water: biolocomotion at the interface. Annu. Rev. Fluid Mech. 2006, 38, 339-369.

(51) Bhushan, B., Jung, Y. C. Natural and biomimetic artificial surfaces for superhydrophobicity, self-cleaning, low adhesion, and drag reduction. Prog. Mater Sci. 2011, 56, 1-108.

Table 1. Surface atomic content of C, O, and Cu detected by XPS on blank sample, modified sample and annealed sample.

At%	C	O	Cu
Blank sample	33.74	43.93	12.42
Modified sample	76.47	16.02	4.86
Annealed sample	32.33	37.41	25.73

Table 2. Contact angles and rolling angles of the prepared surperhydrophobic surface after different cycles of abrasion test

Cycle of abrasion test/time	Contact angle/degree	Rolling angle/degree
0	162±2.1	1±0.2
2	160±2.0	1±0.3
5	159±1.9	3±0.3
10	159±2.1	3±0.4
15	158±2.3	5±0.5
20	146±1.9	22±1.2
Re-modification	146±2.1	21±1.1

Table 3. Contact angles and rolling angles of the prepared surperhydrophobic surface after different time of flush test

Time of flush test/hour	Contact angle/degree	Rolling angle/degree
0	162±2.1	1±0.2
3	161±1.9	2±0.3
6	155±2.1	5±0.5
12	0	-
Re-modification	162±2.1	1±0.2
3	160±1.9	2±0.3
6	156±2.0	5±0.5

Figure 1. SEM images of the surface morphology with different AC etching durations: (A) 0 s (bare brass substrate); (B) 1 min; (C) 5 min; (D) 10 min; (E) & (F) 15 min; (G) 20 min and (H) 30 min, insets are the EDS images of the corresponding surfaces.

Figure 2. (A) TEM image of the prepared $CuO/Cu(OH)_2$ crystals; (B) HRTEM image of the region marked by the white arrow in (A); (C) The electron diffraction pattern of the area marked by the white arrow in (A) (White is for $Cu(OH)_2$ and red is for CuO); (D) XRD patterns of the (a) untreated brass substrate and (b) the AC etching treated substrate. Inset is the high-resolution image of XRD peaks match with $CuO/Cu(OH)_2$.

Figure 3. Mechanism of AC etching of brass substrate in solution containing KOH and $K_2S_2O_8$.

Figure 4. The digital CAs images and the SEM images of the prepared flower-like $CuO/Cu(OH)_2$ nanorods surface (A) before and (B) after modified by myristic acid, and (C) after annealing at 200^{o}C; (D) the schematic diagram of the wetting behavior transition.

Figure 5. The digital CAs images of the (A) blank brass substrate; (B) modified brass substrate; (C) prepared nanorods film substrate and (D) modified nanorods film substrate.

Figure 6. (A) The contact angles of the surface after different annealing time (average of 5 different positions); (B) Cycles between superhydrophobicity and superhydrophilicity of the prepared surface after modification and annealing.

Figure 7. (a)XPS survey spectra and high-resolution spectra of (b) Cu 2p regions, (c) O 1s regions and (d) C 1s regions. (1), (2) and (3) are corresponding to the blank sample, modified sample and annealed sample, respectively.

Figure 8. (A) Digital image of prepared superhydrophobic brass substrate; (B) Digital image of large scale superhydrophobic brass substrate with a curved shape; (C) The schematic diagram of the suggested device: a water drop collecting device based on the prepared large–scale superhydrophobic surface.

Graphical abstract

The digital CAs images and the SEM images of the prepared flower-like nanorods surface (A) before and (B) after modified by myristic acid, and (C) after annealing at 200°C; (D) the schematic diagram of the wetting behavior transition.

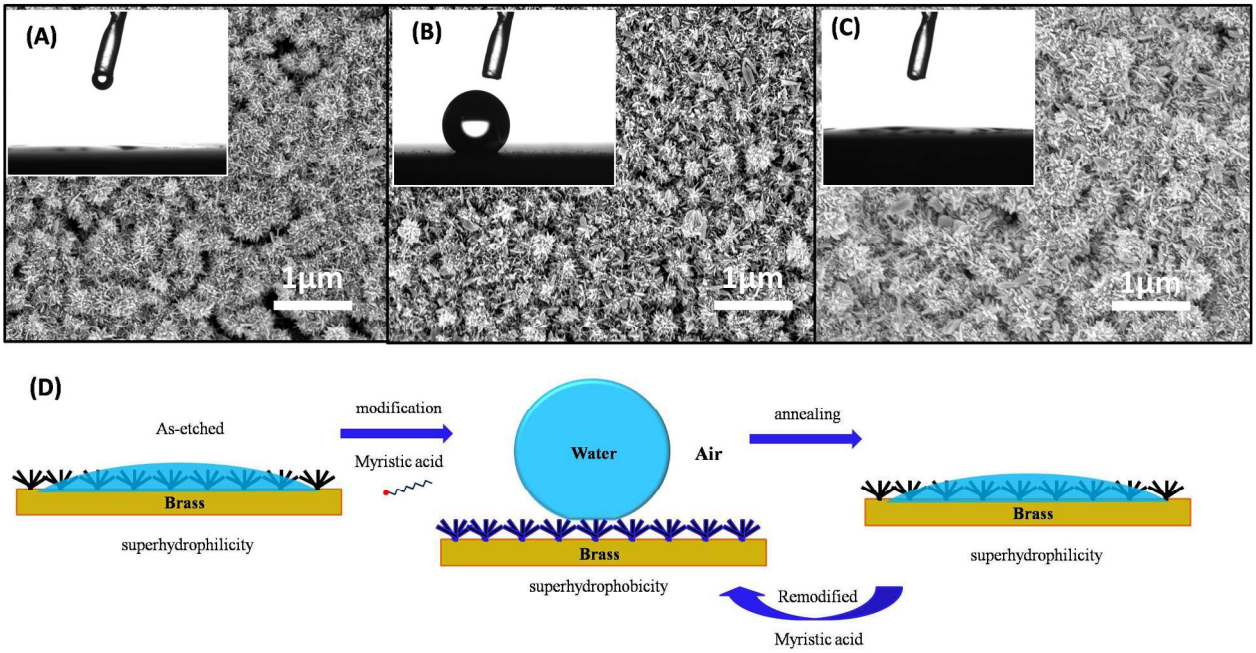

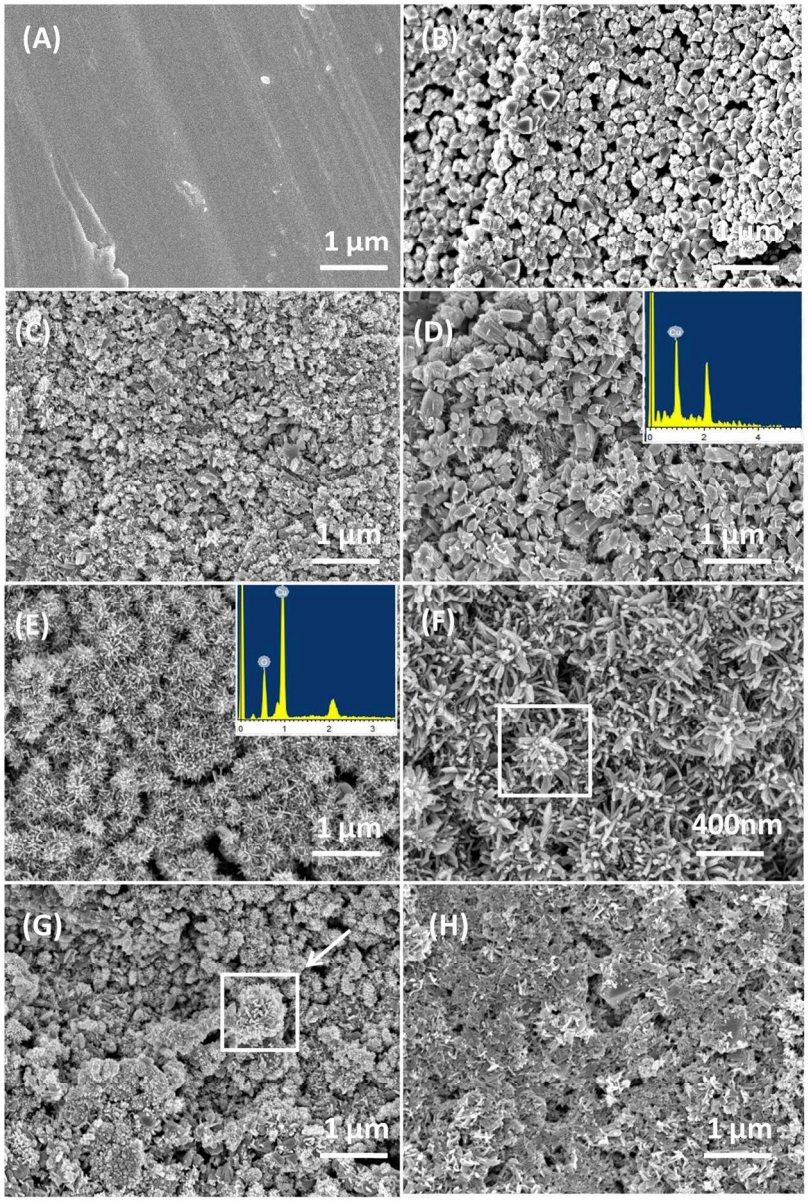

146x215mm (300 x 300 DPI)

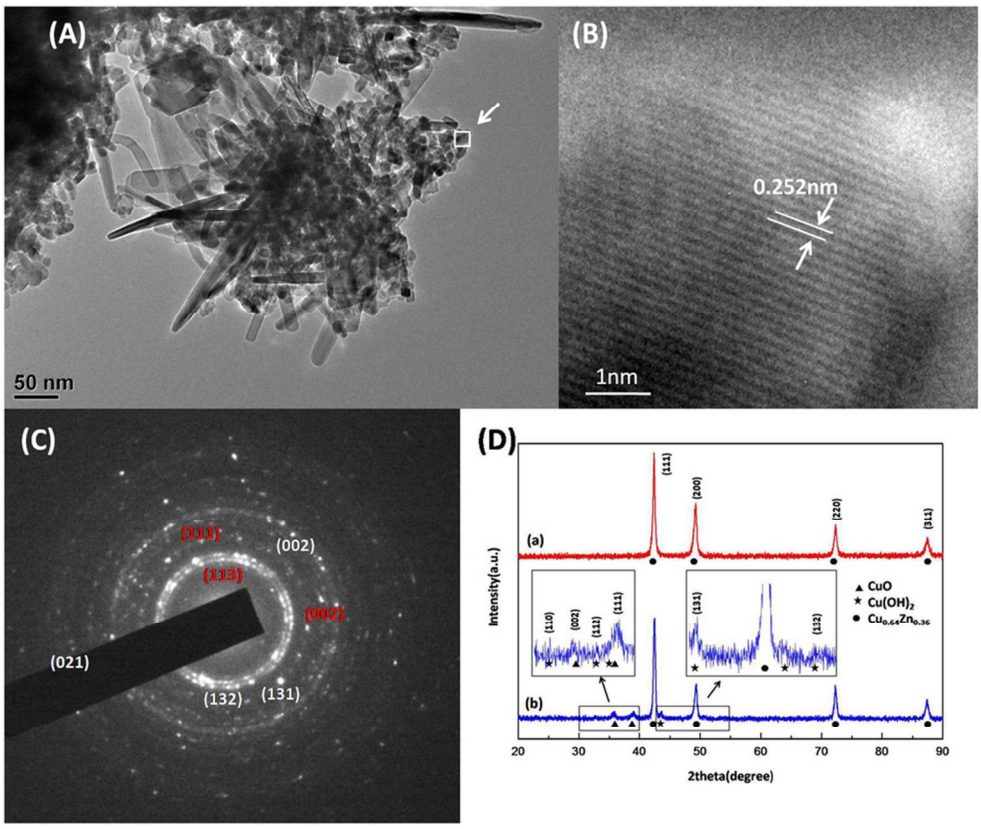

82x68mm (300 x 300 DPI)

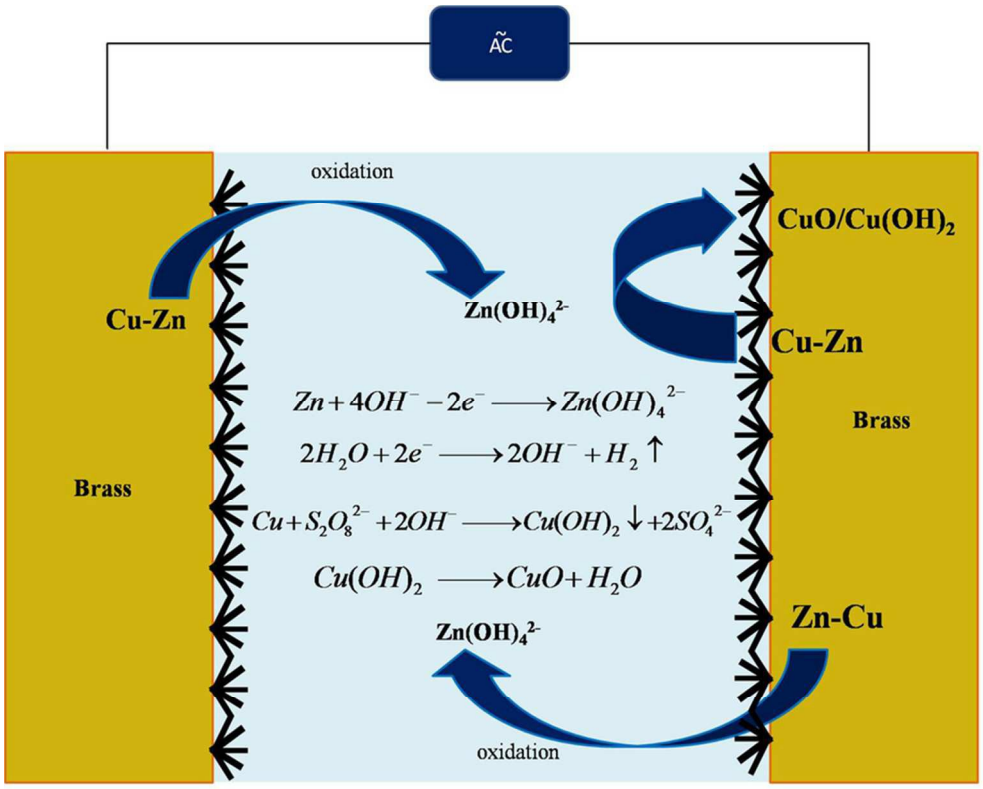

79x62mm (300 x 300 DPI)

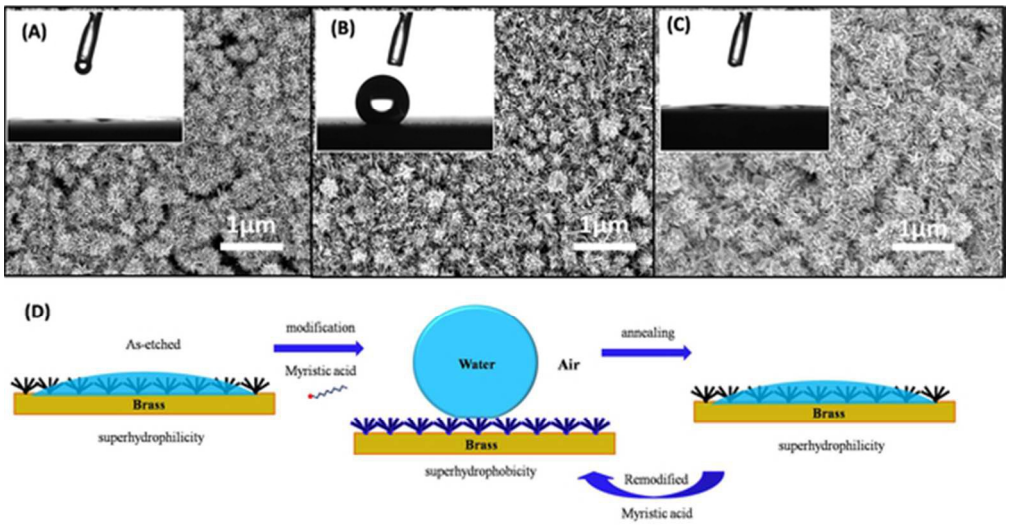

51x27mm (300 x 300 DPI)

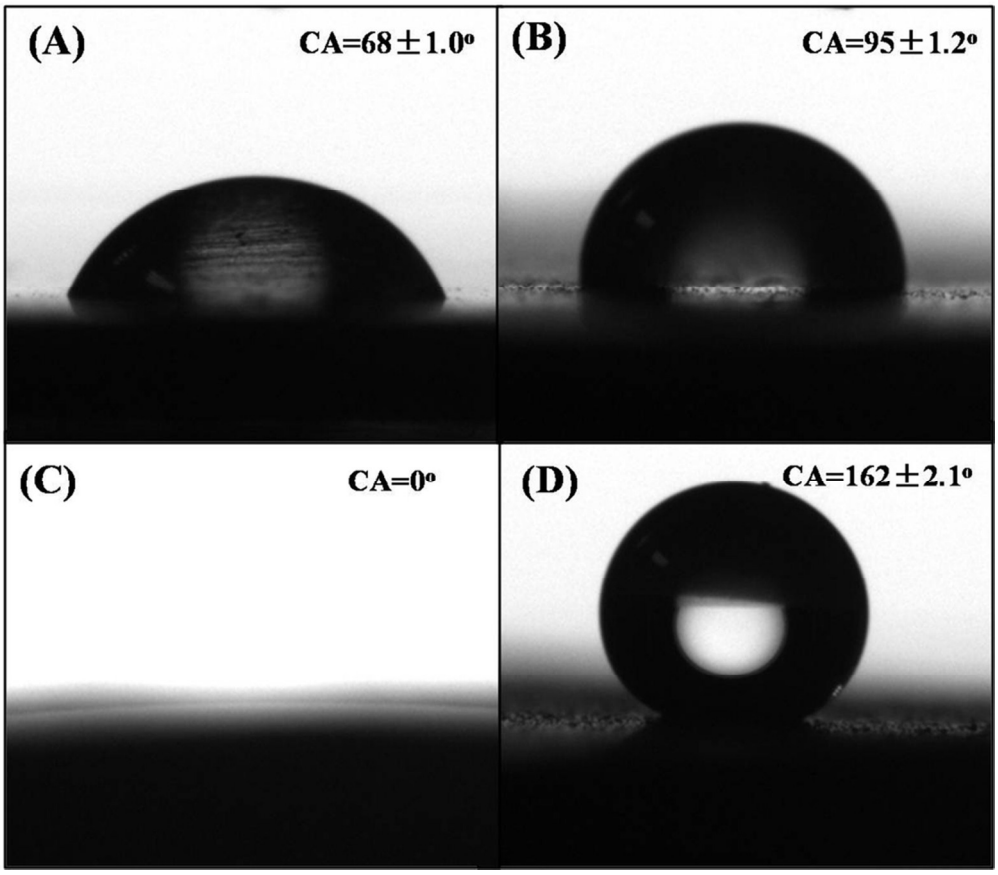

87x76mm (300 x 300 DPI)

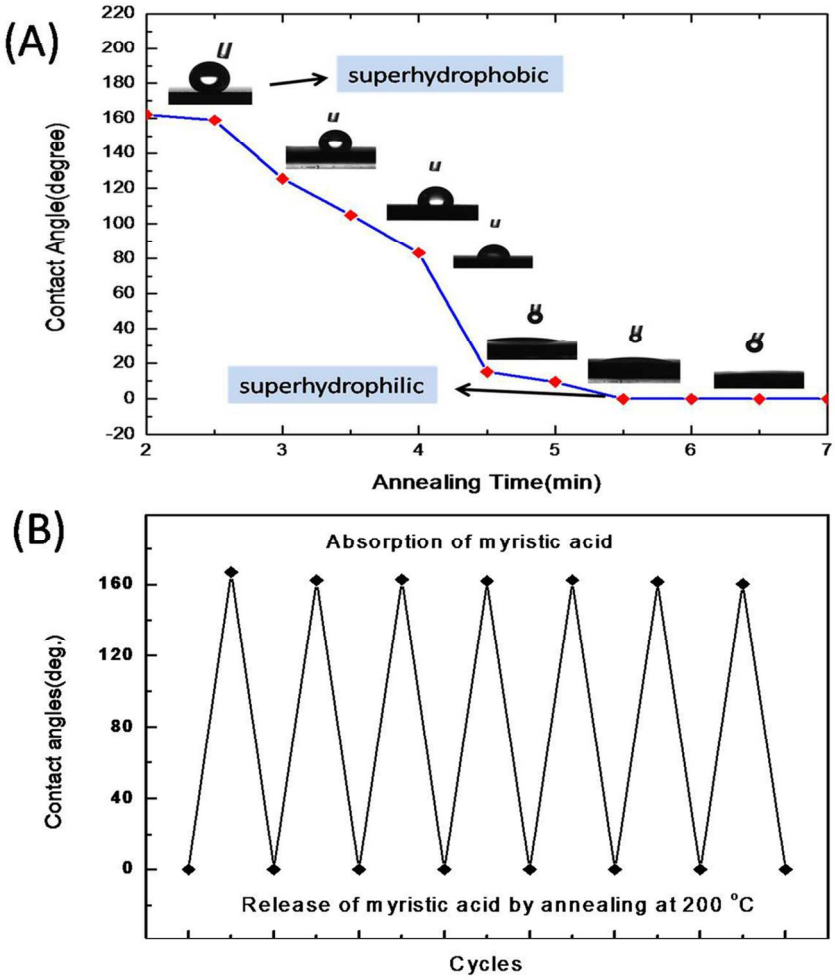

109x119mm (300 x 300 DPI)

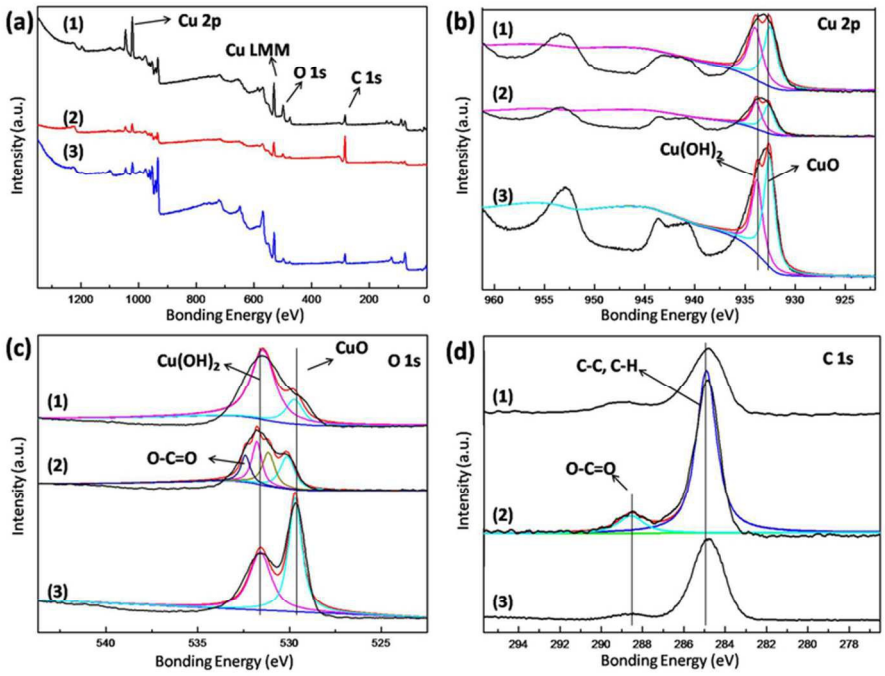

74x55mm (300 x 300 DPI)

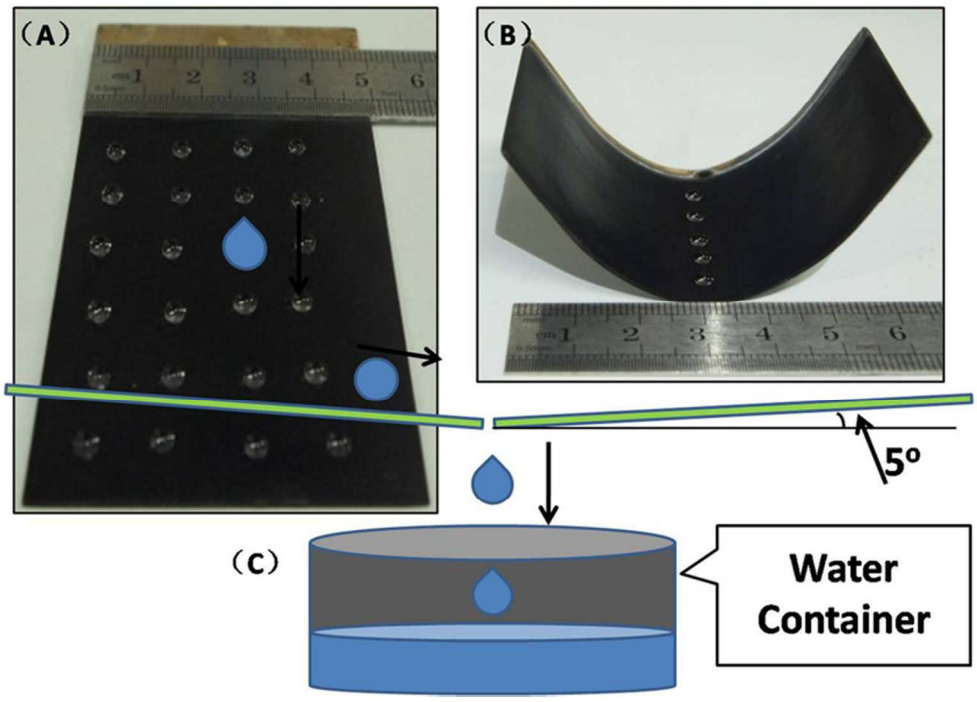

69x48mm (300 x 300 DPI)